Theoretical study of the crystal and electronic properties of α-RuI_3

Yang Zhang,[1] Ling-Fang Lin,[1] Adriana Moreo,[1,2] and Elbio Dagotto[1,2]
[1]*Department of Physics and Astronomy, University of Tennessee, Knoxville, Tennessee 37996, USA*
[2]*Materials Science and Technology Division, Oak Ridge National Laboratory, Oak Ridge, Tennessee 37831, USA*

(Received 3 November 2021; accepted 25 January 2022; published 4 February 2022)

The material α-$RuCl_3$, with a two-dimensional Ru honeycomb sublattice, has attracted considerable attention because it may be a realization of the Kitaev quantum spin liquid. Recently, a new honeycomb material, α-RuI_3, was prepared under moderately high pressure, and it is stable under ambient conditions. However, different from α-$RuCl_3$, α-RuI_3 was reported to be a paramagnetic metal without long-range magnetic order down to 0.35 K. Here, the structural and electronic properties of the quasi-two-dimensional α-RuI_3 are theoretically studied. First, based on first-principles density functional theory calculations, the ABC stacking honeycomb-layer $R\bar{3}$ (No. 148) structure is found to be the most likely stacking order for α-RuI_3 along the c axis. Furthermore, both $R\bar{3}$ and $P\bar{3}1c$ are dynamically stable because no imaginary frequency modes were obtained in the phononic dispersion spectrum without Hubbard U. Moreover, the different physical behavior of α-RuI_3 compared to α-$RuCl_3$ can be understood naturally. The strong hybridization between Ru $4d$ and I $5p$ orbitals decreases the "effective" atomic Hubbard repulsion, leading the electrons of RuI_3 to be less localized than in $RuCl_3$. As a consequence, the effective electronic correlation is reduced from Cl to I, leading to the metallic nature of α-RuI_3. Based on the DFT+U ($U_{\text{eff}} = 2$ eV) plus spin-orbital coupling, we obtained a spin-orbit Mott insulating behavior for α-$RuCl_3$ and, with the same procedure, a metallic behavior for α-RuI_3, in good agreement with experimental results. Furthermore, when introducing large (unrealistic) $U_{\text{eff}} = 6$ eV, the spin-orbit Mott gap opens in α-RuI_3 as well, supporting the physical picture we are proposing. Our results provide guidance to experimentalists and theorists working on two-dimensional transition metal tri-iodide layered materials.

DOI: 10.1103/PhysRevB.105.085107

I. INTRODUCTION

Due to their rich physical properties, low-dimensional materials continue to attract considerable attention in the condensed-matter community [1–19]. In systems with $3d$ transition-metal (TM) atoms, the electronic correlation couplings (i.e., Hubbard repulsion U and Hund's coupling J_H) play a key role in understanding their physical properties. Their spin-orbital coupling (SOC) λ is considered to be negligible. In those compounds, a wide variety of remarkable physical phenomena have been found to be driven by the bandwidth W (corresponding to the kinetic hopping parameter t) and the electronic correlation couplings. The unusual states induced include high-T_c superconductivity [1,20–23], ferroelectricity triggered by spin or charge ordering [24–27], orbital ordering [28–30], and charge or spin density waves [9,31,32].

However, the $4d$ and $5d$ orbitals are more spatially extended than the $3d$ orbitals, leading to increased hopping t in the $4d/5d$ case. Furthermore, U and J_H are also reduced in the $4d/5d$ systems compared to those for $3d$ electrons [33,34]. Moreover, the SOC parameter λ is enhanced in $4d/5d$ systems [35], inducing comparable values of λ with U and J_H. In this case, several intriguing electronic phases have been reported in $4d$ and $5d$ low-dimensional materials. In some dimer systems with $4d$ or $5d$ TM atoms, an interesting orbital-selective Peierls phase could be stable [36,37] when the intrahopping t is larger than the typical Hund's couplings. This phase resembles the previously discussed orbital-selective Mott phase [38–41], but with the localized band induced by a Peierls distortion instead of Hubbard interactions [36,37]. The Hubbard repulsion U can lead to the localization of the spin-orbit coupled pseudospin degrees of freedom, resulting in a "spin-orbit Mott" insulating phase [42–44].

More interestingly, due to the strong bond-dependent anisotropic coupling among spins, a quantum spin liquid (QSL) ground state due to spin quantum fluctuations and frustration is theoretically obtained in the spin-1/2 honeycomb lattice via the Kitaev model [45]. Honeycomb lattice materials with spin-1/2 were proposed to realize the Kitaev physics, such as the $5d^5$ iridates A_2IrO_3 (A = Na, Li) [46–51]. In those systems, the concept of spin-1/2 arises from the effective $J_{\text{eff}} = 1/2$ pseudospins induced by the strong SOC and crystal-field splitting [42]. However, due to substantial lattice distortions, such as dimerization under hydrostatic pressure, the $J_{\text{eff}} = 1/2$ physical picture is destroyed [52,53], and the Kitaev QSL is not realized.

A related Kitaev QSL candidate material is α-$RuCl_3$ with a $4d^5$ electronic configuration analog to the $5d^5$ iridates [54]. This material also forms layered two-dimensional honeycomb structures, and the $4d^5$ electronic configuration of Ru is in a low-spin state with $S = 1/2$, producing $J_{\text{eff}} = 1/2$ pseudospins [55,56]. At ambient conditions, α-$RuCl_3$ exhibits spin-orbital Mott insulating behavior with a zigzag antiferromagnetic (AFM) ordering at 7–13 K [56,57]. Several stacking

 ©2022 American Physical Society

orders have been reported that belong to different space groups, such as $C2/m$ (No. 12) [55,56,58], $P3_112$ (No. 151) [59], and $R\bar{3}$ (No. 148) [60]. Its unconventional interesting behavior, such as highly unusual magnetic excitations, the emergence of Majorana fermions, and a possible Kitaev QSL, has attracted considerable attention in both experiments and theories related to this compound [58,60–70].

Very recently, a new honeycomb-structured material, α-RuI_3, was synthesized at moderately high pressures [71,72]. In general, considering the atomic number of I, the SOC effect should be larger than in Cl, which may lead to more interesting physical properties in RuI_3. Before the experimental preparation of α-RuI_3, there were only a few theoretical studies focusing on the monolayer form [73,74]. Preliminary characterization reveals metallic and paramagnetic behavior, with the absence of long-range magnetic order down to 0.35 K [71,72]. For α-RuI_3 two different stacking orders were reported along the c axis: the $R\bar{3}$ (No. 148) structure with three-layer ABC stacking honeycomb-layer centrosymmetric rhombohedral symmetry [71] and a two-layered honeycomb structure model with space group P_31c (No. 163) [72]. In each RuI_6 plane, the honeycomb layers are built of edge-sharing RuI_6 octahedra. Different from the Ru-Cl bonds in α-$RuCl_3$ [55], the Ru-Ru bonds are identical, with a Ru-Ru bond of length 3.92 Å [71]. The van der Waals (vdW) layer distance is about 6.3 Å, larger than the value for α-$RuCl_3$ (∼5.7 Å) [71], suggesting a weaker interlayer coupling in α-RuI_3 than in α-$RuCl_3$. Then, all current experimental information suggests that α-RuI_3 is different from α-$RuCl_3$.

To better understand the different physical behaviors of α-RuI_3 and α-$RuCl_3$, here, using the density functional theory (DFT), we provide a comprehensive first-principles study of these bulk systems. First, we found the ABC stacking honeycomb-layer $R\bar{3}$ (No. 148) structure is the most likely stacking order of α-RuI_3 along the c axis. Furthermore, both $R\bar{3}$ and $P\bar{3}1c$ are dynamically stable because no imaginary frequency modes were obtained in the phononic dispersion spectrum. In addition, the p-d hybridization increases from Cl to I, leading to the "effective" decrease of the atomic Coulomb repulsion U, resulting in the electrons of RuI_3 being less localized than in $RuCl_3$. The effective electronic correlation is reduced in I to a value not large enough to open the spin-orbit Mott gap in α-RuI_3, leading to its metallic nature. Furthermore, we observed that introducing large (unrealistic) $U_{\text{eff}} = 6$ eV, the spin-orbit Mott gap does open in α-RuI_3, supporting the consistency of the physical picture we proposed.

II. CALCULATION METHOD

In the present study, we performed first-principles DFT calculations using the projector augmented wave method, as implemented in the Vienna *Ab initio* Simulation Package (VASP) code [75–77]. For the electronic correlations, the generalized gradient approximation (GGA) with the Perdew-Burke-Ernzerhof (PBE) potential was employed [78] in our DFT calculations. Our plane-wave cutoff energy was 400 eV. Furthermore, the k-point mesh was appropriately modified for different structures to make the in-plane k-point densities approximately the same in reciprocal space (e.g., $8 \times 8 \times 3$ for the $R\bar{3}$ phase of α-RuI_3). Note that those k-point meshes were tested to confirm that converged energies were produced. Both the lattice constants and atomic positions were fully relaxed until the Hellman-Feynman force on each atom was smaller than 0.01 eV/Å. The phonon spectra were calculated using the finite-displacement approach and were analyzed using the PHONONPY software [79,80]. Moreover, on-site Coulomb interactions were considered by using Dudarev's rotationally invariant DFT+U formulation [81] with $U_{\text{eff}} = U - J = 2$ eV, where this effective U_{eff} is believed to provide an excellent description of α-$RuCl_3$ [82]. It should be noted that hybrid exchange-correlation functionals, such as B3LYP (Becke, 3-parameter, Lee-Yang-Parr), allow us to achieve excellent agreement with experiments for the band gaps of complex oxide materials [83,84], whereas the DFT technique usually underestimates the band gaps. The hybrid exchange-correlation functional provides only a correction for the band gap and does not change other physical properties. However, the scope of this publication is to focus on the physical properties of the metallic phase of RuI_3. Hence, our DFT+U calculations are good enough to qualitatively describe the system we focus on. All the crystal structures were visualized with the VESTA code [85].

TABLE I. The optimized lattice constants (Å) of the $R\bar{3}$ (No. 148) structure of α-RuI_3, using the PBE, PBE+D3, PBE+D3, PBEsol, PBEsol+D3, and PBEsol+D3(BJ) methods. The experimental values (Expt. for short) are also listed for comparison and were reported to form the $R\bar{3}$ (No. 148) structure [71]. Note that D3 denotes vdW-D3 with zero damping and D3(BJ) denotes vdW-D3 with Becke-Jonson damping.

	a	b	c
PBE	6.957	6.957	20.369
PBE+D3	6.875	6.875	18.841
PBE+D3(BJ)	6.817	6.817	18.301
PBEsol	6.821	6.821	18.487
PBEsol+D3	6.761	6.761	17.918
PBEsol+D3(BJ)	6.695	6.695	17.393
Expt.	6.791	6.791	19.026

Based on the $R\bar{3}$ (No. 148) structure of α-RuI_3, we compared the results of optimized crystal structures using different exchange-correlation functionals with or without vdW interactions, including PBE [78], PBE functional revised for solids (PBEsol) [86], zero damping vdW DFT-D3 corrections of Grimme (vdW-D3) [87], and vdW-D3 with Becke-Jonson damping [88]. As shown in Table I, all the obtained in-plane lattice constants of different exchange-correlation functionals are close to the experimental values, with the largest discrepancy being 2.4% for the a value in PBE. But the PBE+vdW-D3 with zero damping functional provides the most accurate description for the c axis (a 1% difference from the experimental value). Furthermore, the obtained in-plane lattices of the PBE+vdW-D3 with zero damping functional are only 1.2% larger than experimental results. Hence, we use the PBE+D3 with zero damping method in the structural optimization of the bulk properties in the rest of the paper.

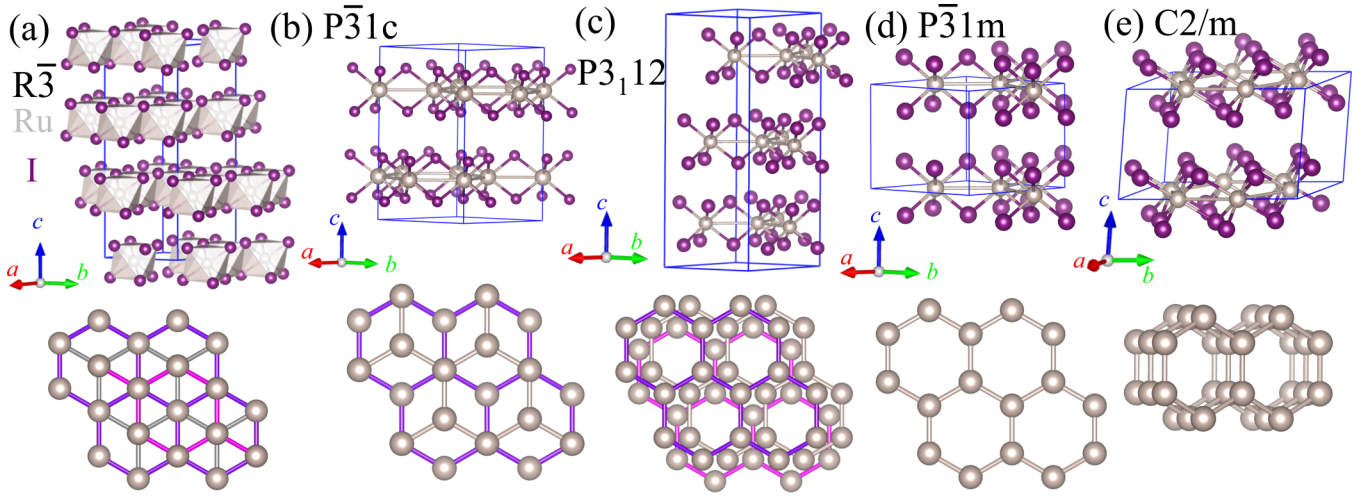


FIG. 1. Five different conventional cells (gray = Ru; purple = I) with one-, two-, and three-layer periodicity along the c axis. The lower panels display the schematic view of three Ru honeycomb lattices for crystal structures. Solid blue lines in the top panels depict conventional cells. (a) $R\bar{3}$ (No. 148), (b) $P\bar{3}1c$ (No. 163), (c) $P3_112$ (No. 151), (d) $P\bar{3}1m$ (No. 162), and (e) $C2/m$ (No. 12).

III. RESULTS

A. Stacking order of α-RuI_3 along the c axis

First, let us discuss the stacking order of α-RuI_3. Five stacking configurations were considered in our study, as shown in Fig. 1, where the lower panels display the top view of the Ru honeycomb sublattice. The main difference between those five structures is the different stacking orderings along the c axis. The $R\bar{3}$, $P3_112$, and $C2/m$ structures involve three-layer periodicity stacking, resulting in three Ru honeycomb sublattices stacking, as shown in the lower panels in Fig. 1. Note that the monoclinic $C2/m$ structure was reported to be the crystal structure of α-$RuCl_3$ [55] with in-plane shifting of the Ru honeycomb stacking, and it is similar to space group $P3_112$, which was also suggested to be the space group of α-$RuCl_3$ [59]. The $P\bar{3}1m$ and $P\bar{3}1c$ structures involve only one- and two-layer periodicity along the c axis. Note that both $R\bar{3}$ and $P\bar{3}1c$ structures were shown experimentally to be the space group of α-RuI_3 [71,72]. Furthermore, Ru-Ru dimerization was reported experimentally in the $C2/m$ and $P3_112$ structures of α-$RuCl_3$ [55,59].

Our optimized lattice constants are $a = b = 6.875$, $c = 18.841$ Å and $a = b = 6.873$, $c = 12.577$ Å for $R\bar{3}$ (No. 148) and $P\bar{3}1c$ (No. 163), respectively, which are close to the experimental results ($a = b = 6.791$, $c = 19.026$ Å for $R\bar{3}$ and $a = b = 6.778$, $c = 12.579$ Å for $P\bar{3}1c$) [71,72]. Based on the optimized structures, we calculated their relative total energies with GGA in the nonmagnetic state as summarized in Table II. We found that the $R\bar{3}$ (No. 148) configuration has the lowest energy, indicating this stacking structure is the most likely stacking order among all the candidates. Note that here, we do not consider nuclear quantum effects. Based on our results, the proper conclusion is that $R\bar{3}$ (No. 148) is the most possible ground state in the *absence* of nuclear quantum effects. However, this could change with the inclusion of those nuclear quantum effects, and consequently, a final determination is left to future work. The $P\bar{3}1c$ structure has a slightly higher energy than the $R\bar{3}$ structure.

To better understand the structural stability of α-RuI_3, we carried out the phononic dispersion calculations using a $2 \times 2 \times 1$ supercell for the $R\bar{3}$ (No. 148) and $P\bar{3}1c$ (No. 163) phases. Figure 2 indicates that the $R\bar{3}$ and $P\bar{3}1c$ structures are dynamically stable because no imaginary frequency modes were obtained in the phononic dispersion spectrum.

In addition, we also considered the Coulombic repulsion U effect on the process of optimizing crystal lattices (see Table S1 in the Supplemental Material [89]). The lattice structures do not change much compared to the lattice structures without U_{eff}, and the $R\bar{3}$ structure of α-RuI_3 has the lowest energy among those five lattice configurations. Furthermore, we also compared the energies between the $R\bar{3}$ and $P\bar{3}1c$ structures with and without the effective Coulomb repulsion U effect, considering the experimentally reported lattice structures where $R\bar{3}$ α-RuI_3 always has lower energy than $P\bar{3}1c$ α-RuI_3. Moreover, we also calculated the phononic dispersion with $U_{\text{eff}} = 2.0$ eV for both the $R\bar{3}$ and $P\bar{3}1c$ phases. We found that the $R\bar{3}$ phase is dynamically stable because no imaginary frequency modes were obtained in the phononic dispersion spectrum. However, the phononic dispersion spectrum of

TABLE II. Optimized lattice constants (Å) and energy differences (meV/Ru) with respect to the $R\bar{3}$ (No. 148) configuration taken as the reference of energy for the various structural configurations. The experimental values (Expt. for short) are also listed for comparison, which were reported to form the $R\bar{3}$ (No. 148) [71] and $P\bar{3}1c$ (No. 163) structures [72].

	a	b	c	Energy
$R\bar{3}$ (No. 148)	6.875	6.875	18.841	0
$P\bar{3}1c$ (No. 163)	6.873	6.873	12.577	2.58
$P3_112$ (No. 151)	6.841	6.841	19.209	6.35
$P\bar{3}1m$ (No. 162)	6.828	6.828	6.413	25.83
$C2/m$ (No. 12)	6.865	11.827	6.764	7.68
Expt. [71]	6.791	6.791	19.026	
Expt. [72]	6.778	6.778	12.579	

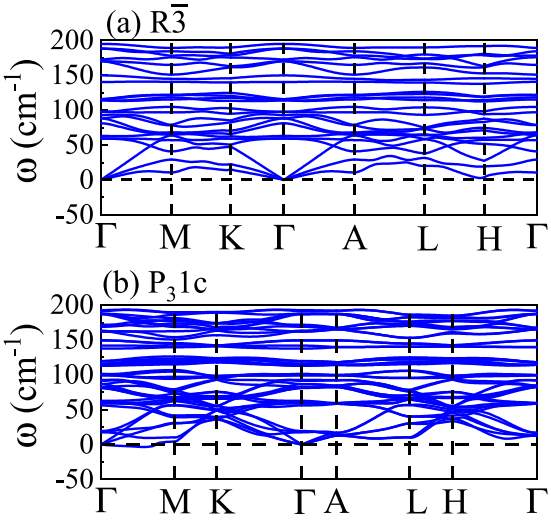


FIG. 2. The calculated phonon spectrum of α-RuI_3 for the structures (a) $R\bar{3}$ and (b) $P\bar{3}1c$ in the nonmagnetic state without Hubbard U. The coordinates of the high-symmetry points in the bulk Brillouin zone (BZ) are $\Gamma = (0, 0, 0)$, $M = (0.5, 0, 0)$, $K = (1/3, 1/3, 0)$, $A = (0, 0, 0.5)$, $L = (0.5, 0, 0)$, and $H = (1/3, 1/3, 0.5)$.

$P\bar{3}1c$ suggests that this structure is unstable, as displayed in Fig. S1(b). In this case, the electronic correlation effects may induce a structural phase transition for the $P\bar{3}1c$ case. Since the energy difference of these two structures is quite small, a possible structural phase transition at finite temperatures deserves further experimental investigation and discussion beyond the scope of our present paper. Hence, based on our DFT calculations, we believe that the $R\bar{3}$ structure is the most likely crystal structure of α-RuI_3. It should also be noted that $R\bar{3}$ and $P\bar{3}1c$ have quite similar crystal and electronic structures. The metallic behavior and strong p-d hybridizations are also obtained in the $P\bar{3}1c$ structure of α-RuI_3 (see Figs. S3 and S4).

For the benefit of our readers, we also present the corresponding electronic structures of $P\bar{3}1c$ α-RuI_3 in the Supplemental Material [89]. We also remark that the main physical conclusion of our paper is not affected by the structural configurations because the difference between those structures is the stacking arrangement along the c axis. In the rest of the text, we will focus on discussing the results for $R\bar{3}$ α-RuI_3, starting in the next section.

B. Electronic structures.

Let us now discuss the energy splitting of the Ru $4d^5$ orbitals, as sketched in Fig. 3(a). First, the crystal field leads to three lower-degenerate-energy t_{2g} orbitals (d_{xy}, d_{yz}, and d_{xz}) and two higher-degenerate-energy e_g orbitals ($d_{x^2-y^2}$ and $d_{3z^2-r^2}$). In addition, by introducing the SOC effect, the three lower-degenerate-energy t_{2g} orbitals split into two energy states, $J_{\rm eff} = 3/2$ and $J_{\rm eff} = 1/2$. The Ru^{3+} state is considered a d^5 electronic configuration with a low-spin state. Thus, this system could be regarded as a $J = 1/2$ state (half-occupied $J_{\rm eff} = 1/2$ state), while the two $J_{\rm eff} = 3/2$ states are fully occupied, as shown in Fig. 3(a).

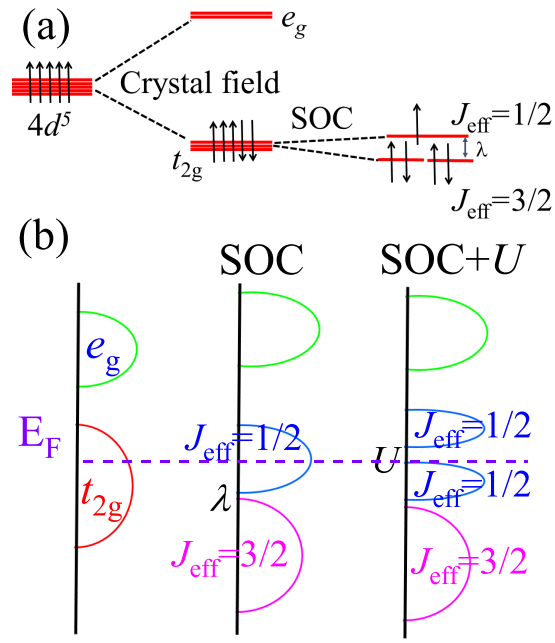


FIG. 3. (a) Schematic energy splitting of the Ru $4d$ orbitals in the d^5 low-spin configuration. (b) Schematic of the local density of states for the cases without interactions, with only SOC, and with both SOC and U in this Ru $4d^5$ configuration.

In general, the density of states (DOS) of this $4d^5$ low-spin configuration can be intuitively understood as displayed in Fig. 3(b). Under a cubic crystal field, the five $4d$ electrons of Ru populate the lower t_{2g} bands separated by the crystal-field splitting energy (∼10 Dq), resulting in a metallic phase because the t_{2g} orbitals are not completely occupied. Then, by introducing the SOC effect, the $J_{\rm eff} = 1/2$ and $J_{\rm eff} = 3/2$ states begin to separate from each other, leading to a half-occupied $J_{\rm eff} = 1/2$ state and two fully occupied $J_{\rm eff} = 3/2$ states, where the splitting energy depends on the SOC strength λ. In this case, the system is still metallic since the $J_{\rm eff} = 1/2$ state is not completely occupied. Finally, increasing the on-site electronic correlations U leads to an energy gap for the $J_{\rm eff} = 1/2$ band near its Fermi surface as well, resulting in a Mott transition. In this case, this insulating gap system is also often referred to as the "spin-orbit Mott insulating" gap.

To better understand the similarities and differences between α-RuI_3 and α-$RuCl_3$, we calculated the DOSs of α-RuI_3 with the $R\bar{3}$ structure and α-$RuCl_3$ with the $C2/m$ structure for the nonmagnetic phase. According to the calculated DOSs [see Figs. 4(a) and 4(b)], the bands near the Fermi level are mainly contributed by the Ru $4d$ t_{2g} orbitals, *hybridized* with the I $5p$ and Cl $3p$ orbitals, respectively. Furthermore, the I $5p$ orbitals are closer to the Fermi level than the Cl $3p$ orbitals, as shown in Figs. 4(a) and 4(b). With increasing atomic radius from Cl to I, the p components near the Fermi level become larger, leading to an increase in the p-d hybridization tendency from I to Cl. In addition, the low-energy t_{2g} bands are more extended in α-RuI_3 than in α-$RuCl_3$, indicating stronger electronic correlations (U/W, where W is the bandwidth) in the α-$RuCl_3$ case. To open the Mott gap in the $J_{\rm eff} = 1/2$ state, α-RuI_3 needs a larger

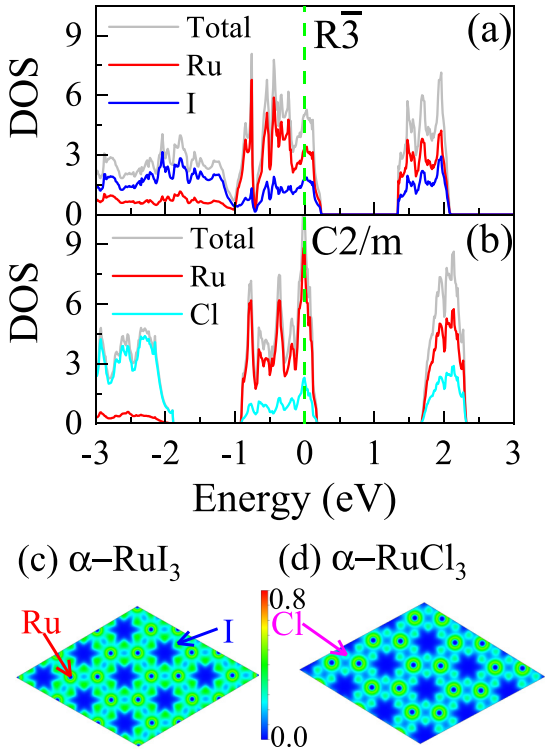


FIG. 4. (a) and (b) Density of states near the Fermi level based on the nonmagnetic states for α-RuI_3 and α-$RuCl_3$, respectively. Gray: total; red: Ru; blue: I; cyan: Cl. The Fermi level is marked by the vertical dashed green line. (a) Results for the $R\bar{3}$ structure of α-RuI_3. (b) Results for the $C2/m$ structure of α-$RuCl_3$. (c) and (d) Electron localization function of one Ru honeycomb layer for α-RuI_3 and α-$RuCl_3$, respectively, corresponding to nonmagnetic phases, in the a-b plane.

Coulomb repulsion U than α-$RuCl_3$. It should be noted that those results are obtained in the $P\bar{3}1c$ structure of α-RuI_3 and the $P3_112$ structure of α-$RuCl_3$ (see the Supplemental Material [89]).

In addition, we also calculated the electron localization function (ELF) [90] for the α-RuI_3 and α-$RuCl_3$ cases, as displayed in Figs. 4(c) and 4(d), respectively. The ELF picture indicates that the charges are less localized inside the Ru-I bonds, resulting in large hybridized p-d bonds in α-RuI_3, in contrast to the localized charges along with the Ru-Cl bonds in α-$RuCl_3$. The movement of electrons is by tunneling from Ru to I (or Cl) and then to another Ru. In other words, iodine (or chlorine) is the bridge between rutheniums. Hence, it is easy to imagine that $RuCl_3$ is more Mott localized than RuI_3 by using the same value of the on-site repulsion U at the Ru site. The reason is that compared to $RuCl_3$, the bandwidth of RuI_3 is increased, indicating that the electronic correlation U/W has decreased. In this case, due to the increase in the p-d hybridization of α-RuI_3, the "effective" Coulomb repulsion U/W will decrease in α-RuI_3, reducing or not even permitting the opening of an energy gap. Hence, RuI_3 displays metallic behavior, in contrast to the insulating behavior in α-$RuCl_3$.

Furthermore, we calculated band structures of $R\bar{3}$ α-RuI_3 with and without the SOC effect and with the Coulomb repulsion U ($U_{\text{eff}} = 2$ eV). As shown in Fig. 5, band structures both with and without SOC suggest metallic behavior in α-RuI_3. Taking into account SOC and the Coulomb repulsion U ($U_{\text{eff}} = 2$ eV), α-RuI_3 *still* displays metallic behavior of the $J_{\text{eff}} = 1/2$ bands but opens gaps on some high-symmetry points in the Brillouin zone, as displayed in Fig. 5(b). Those results are consistent with our previous analysis that the effective Coulomb repulsion would reduce or not even allow the gap to open in α-RuI_3. For comparison, we also calculated the band structure of α-$RuCl_3$ using the $C2/m$ structure with and without the SOC effect and with the Coulomb repulsion U ($U_{\text{eff}} = 2$ eV). As displayed in Fig. 6, the band structure clearly shows insulating behavior for the $J_{\text{eff}} = 1/2$ bands with a Mott transition caused by the Coulomb repulsion U. Based on our estimation, the spin-orbital couplings are about 0.12 and 0.2 eV for $RuCl_3$

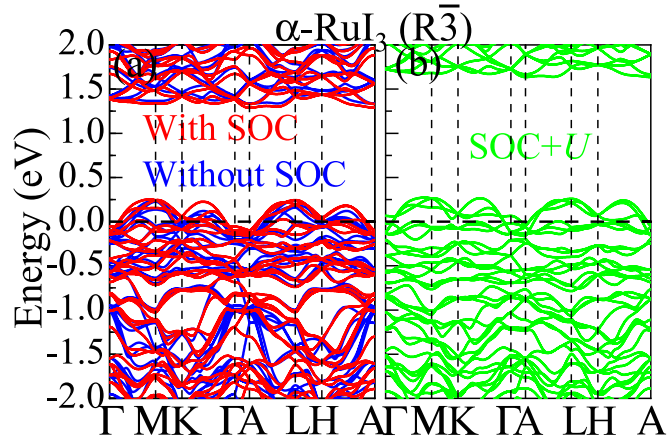


FIG. 5. Calculated electronic band structures of α-RuI_3 in the $R\bar{3}$ structure using a nonmagnetic state: (a) without and with SOC (the color convention is indicated) and (b) with SOC plus $U_{\text{eff}} = 2$ eV. The coordinates of the high-symmetry points in the bulk BZ are $\Gamma = (0, 0, 0)$, $M = (0.5, 0, 0)$, $K = (1/3, 1/3, 0)$, $A = (0, 0, 0.5)$, $L = (0.5, 0, 0)$, and $H = (1/3, 1/3, 0.5)$.

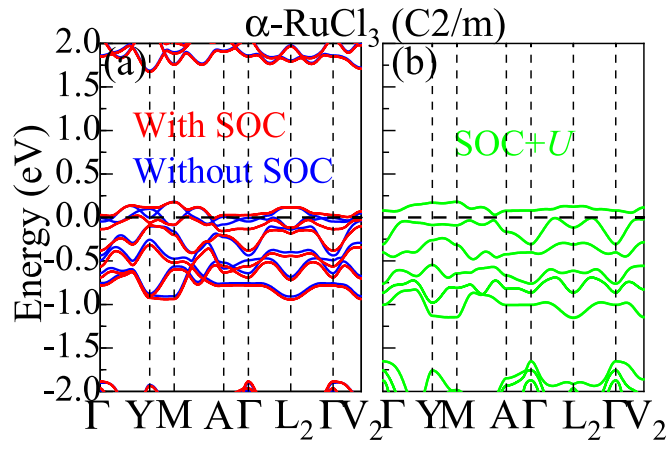


FIG. 6. Calculated electronic band structures of α-$RuCl_3$ with the $C2/m$ structure in the nonmagnetic state: (a) without and with SOC (the color convention is indicated) and (b) with SOC plus $U_{\text{eff}} = 2$ eV. The coordinates of the high-symmetry points in the bulk BZ are $\Gamma = (0, 0, 0)$, $Y = (0.5, 0.5, 0)$, $M = (0.5, 0.5, 0.5)$, $A = (0, 0, 0.5)$, $L_2 = (0, 0.5, 0.5)$, and $V_2 = (0, 0.5, 0)$.

and RuI_3, respectively, in agreement with other theoretical studies [61,72]. Hence, after using suitable parameters, we obtained metallic behavior in α-RuI_3 and insulating behavior in α-$RuCl_3$, in excellent agreement with the experimental results. This can be naturally explained in simple terms: increasing the *p-d* hybridization of α-RuI_3 decreases the effective electronic correlations U/W because the bandwidth W increases and thus allows for the conduction of charge along with the Ru-I bonds.

C. Comparing α-RuI_3 with α-$RuCl_3$ using zigzag AFM order

Preliminary experimental characterization of α-RuI_3 reveals the absence of long-range magnetic order down to 0.35 K, suggesting a paramagnetic metallic state [71,72]. On the contrary, α-$RuCl_3$ is in a spin-orbital Mott state with zigzag AFM ordering in the ground state at low temperatures [56,57]. To better understand the different conductive behaviors of α-RuI_3 and α-$RuCl_3$, we calculated the electronic structures for the two materials assuming zigzag AFM order. Because we are simply performing a qualitative analysis of the effect of the Coulomb repulsion U, we used the $C2/m$ symmetry for the crystal structure for both α-RuI_3 and α-$RuCl_3$.

Based on previous studies [54,56,61,91], U_{eff} has been estimated to be about 1–2 eV for Ru atoms, which are often used in the band structure calculations of trihalogen ruthenium compounds. In addition, the effective $U_{\text{eff}} = 2.0$ eV is believed to provide an excellent description of the stacking order of $RuCl_3$ [82]. Hence, we used $U_{\text{eff}} = 2.0$ eV in our magnetic calculations. Note that we also tested other values of U_{eff}, but they do not change our main conclusion [89]. Furthermore, for $RuCl_3$, previous optical data found a small optical gap of about 0.3 eV [92], but this very small value was considered not to be associated with charge excitations [93]. Moreover, some other experiments suggested that the optical gap was around 1 eV [54,93]. Hence, our results are in good agreement with the optical data for α-$RuCl_3$ qualitatively. Figure 7 indicates that α-RuI_3 still displays metallic behavior, in contrast to the insulating behavior in α-$RuCl_3$. The same SOC + U ($U_{\text{eff}} =$ 2 eV) opens a gap (∼0.7 eV) in α-$RuCl_3$ but could not open the Mott gap in α-RuI_3. This result supports the notion that the effective electronic correlation U/W is reduced from Cl to I and is not enough to open a gap, leading to metallic behavior in α-RuI_3. In this case, the results obtained, even including the effect of Coulomb repulsion, can naturally explain the metallic behavior in α-RuI_3, in contrast to the spin-orbit Mott insulating behavior observed in α-$RuCl_3$.

As discussed in the previous sections, the metallic nature of α-RuI_3 is induced by the reduced effective Coulomb repulsion when moving from Cl to I. In essence, the spin-orbit Mott gap opens if U is large enough. In this case, the Coulomb repulsion U of the Ru atoms shifts Ru states to lower energies and reduces the *p-d* hybridization and thus its bandwidth. To confirm this physical picture, we introduced artificially large (unrealistic) $U_{\text{eff}} = 6$ eV on the Ru sites. This U_{eff} is too large for RuI_3. As expected, using the same lattice as in Fig. 7(a), a large spin-orbit Mott gap (∼1.1 eV) emerges, this time in the DOS, as displayed in Fig. 8. These results support our physical picture for the explanation of the metallic behavior in RuI_3. Note that here, we did only a qualitative analysis

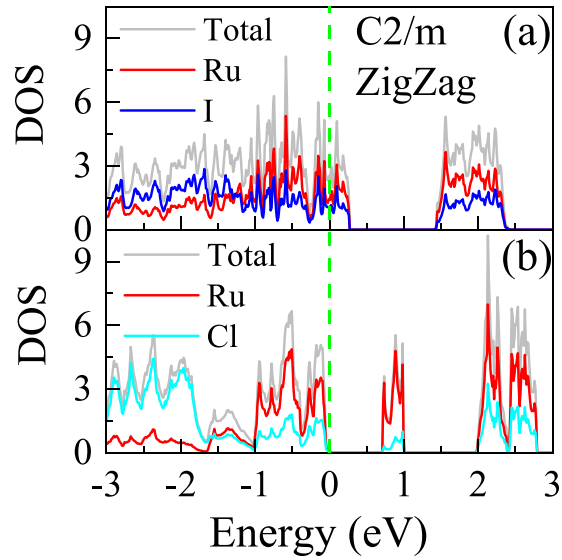


FIG. 7. Density of states near the Fermi level for the zigzag AFM state using the $C2/m$ structure for both α-RuI_3 and α-$RuCl_3$ and with SOC plus U ($U_{\text{eff}} = 2$ eV) for both materials. Gray: total; red: Ru; blue: I; cyan: Cl. The Fermi level is marked by the green dashed line. (a) α-RuI_3, where the Fermi level is inside the valence band, and (b) α-$RuCl_3$, where the Fermi level is inside the gap.

for the metallic-insulating transition of RuI_3 because finding the specific critical value of the Hubbard repulsion U is also affected by many other aspects besides U, such as the lattice structure, magnetic ordering, spin orientation, etc. However, our results are qualitatively sufficient to show that for a large enough U_{eff} a spin-orbit Mott gap opens even in α-RuI_3.

IV. CONCLUSIONS

In this paper, we have systematically studied the properties of α-RuI_3 and α-$RuCl_3$ by using first-principles DFT. We found that the most likely stacking order of α-RuI_3 along the

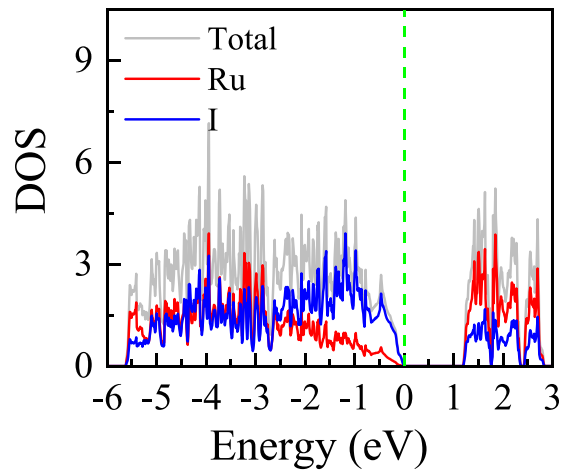


FIG. 8. Density of states near the Fermi level using a zigzag AFM state and the structure $C2/m$ for α-RuI_3 with GGA + SOC + U (employing an unphysically large $U_{\text{eff}} = 6$ eV). Gray: total; red: Ru; blue: I. The Fermi level is marked by the green dashed vertical line.

c axis is the ABC stacking honeycomb-layer $R\bar{3}$ (No. 148) structure. In addition, both $R\bar{3}$ and $P\bar{3}1c$ were found to be dynamically stable because no imaginary frequency modes were obtained in the phononic dispersion spectrum. By introducing GGA + SOC + U calculations, the $J_{\text{eff}} = 1/2$ physics was obtained in both α-RuI_3 and α-$RuCl_3$. Different from the spin-orbit Mott insulating phase of α-$RuCl_3$, on the other hand, α-RuI_3 displays a strong metallic behavior, in agreement with the currently available experimental information. The strong hybridization between the Ru $4d$ and I $5p$ orbitals decreases the effective atomic Coulomb repulsion U/W, that is, increases the bandwidth W in the ratio U/W. This effective electronic correlation U/W is reduced from Cl to I, inducing metallic behavior in α-RuI_3. In our study, by considering large (unrealistic) $U_{\text{eff}} = 6$ eV, the spin-orbit Mott gap finally opens in α-RuI_3, supporting the physical picture we proposed. In summary, while the atomic U of Ru must be very similar in both compounds, the bandwidth W in the case of Cl is smaller than in I, and this is sufficient to place α-$RuCl_3$ on the insulating side of the metal-insulator transition, while α-RuI_3 is still on the metallic side.

ACKNOWLEDGMENTS

The work of Y.Z., L.-F.L., A.M., and E.D. was supported by the U.S. Department of Energy (DOE), Office of Science, Basic Energy Sciences (BES), Materials Sciences and Engineering Division. All the calculations were carried out at the Advanced Computing Facility (ACF) of the University of Tennessee, Knoxville (UTK).

[1] J. G. Bednorz and K. A. Müller, Z. Phys. B **64**, 189 (1986).
[2] E. Dagotto, Rev. Mod. Phys. **66**, 763 (1994).
[3] G. R. Stewart, Rev. Mod. Phys. **83**, 1589 (2011).
[4] E. Dagotto, T. Hotta, and A. Moreo, Phys. Rep. **344**, 1 (2001).
[5] E. Dagotto, Science **309**, 257 (2005).
[6] M. Grioni, S. Pons, and E. Frantzeskakis, J. Phys.: Condens. Matter **21**, 023201 (2009).
[7] D. J. Scalapino, Rev. Mod. Phys. **84**, 1383 (2012).
[8] E. Dagotto, Rev. Mod. Phys. **85**, 849 (2013).
[9] P. Monceau, Adv. Phys. **61**, 325 (2012).
[10] L. F. Lin, Y. Zhang, A. Moreo, E. Dagotto, and S. Dong, Phys. Rev. Materials **3**, 111401(R) (2019).
[11] L. F. Lin, Y. Zhang, A. Moreo, E. Dagotto, and S. Dong, Phys. Rev. Lett. **123**, 067601 (2019).
[12] T. Miao *et al.* Proc. Natl. Acad. Sci. USA **117**, 7090 (2020).
[13] Y. Zhu *et al.* Phys. Rev. B **102**, 235107 (2020).
[14] C. Sen and E. Dagotto, Phys. Rev. B **102**, 035126 (2020).
[15] Y. Zhang, L. F. Lin, A. Moreo, G. Alvarez, and E. Dagotto, Phys. Rev. B **103**, L121114 (2021).
[16] L. F. Lin, Y. Zhang, G. Alvarez, A. Moreo, and E. Dagotto, Phys. Rev. Lett. **127**, 077204 (2021).
[17] A. R. Mazza, E. Skoropata, J. Lapano, J. Zhang, Y. Sharma, B. L. Musico, V. Keppens, Z. Gai, M. J. Brahlek, A. Moreo, D. A. Gilbert, E. Dagotto, and T. Z. Ward, Phys. Rev. B **104**, 094204 (2021).
[18] Y. Zhang, L.-F. Lin, G. Alvarez, A. Moreo, and E. Dagotto, Phys. Rev. B **104**, 125122 (2021).
[19] L.-F. Lin, N. Kaushal, C. Sen, A. D. Christianson, A. Moreo, and E. Dagotto, Phys. Rev. B **103**, 184414 (2021).
[20] Y. Kamihara, T. Watanabe, M. Hirano, and H. Hosono, J. Am. Chem. Soc. **130**, 3296 (2008).
[21] P. C. Dai, J. P. Hu, and E. Dagotto, Nat. Phys. **8**, 709 (2012).
[22] D. Li, K. Lee, B. Y. Wang, M. Osada, S. Crossley, H. R. Lee, Y. Cui, Yi, Y. Hikita, and H. Y. Hwang, Nature (London) **572**, 624 (2019).
[23] Y. Zhang, L.-F. Lin, W. Hu, A. Moreo, S. Dong, and E. Dagotto, Phys. Rev. B **102**, 195117 (2020).
[24] J. van den Brink and D. I. Khomskii, J. Phys.: Condens. Matter **20**, 434217 (2008).
[25] L.-F. Lin, Q.-R. Xu, Y. Zhang, J.-J. Zhang, Y.-P. Liang, and S. Dong, Phys. Rev. Materials **1**, 071401(R) (2017).
[26] S. Dong, H.-J. Xiang, and E. Dagotto, Nat. Sci. Rev. **6**, 629 (2019).
[27] Y. Zhang, L. F. Lin, A. Moreo, S. Dong, and E. Dagotto, Phys. Rev. B **101**, 144417 (2020).
[28] Y. Tokura and N. Nagaosa, Science **288**, 462 (2000).
[29] B. Pandey, Y. Zhang, N. Kaushal, R. Soni, L.-F. Lin, W.-J. Hu, G. Alvarez, and E. Dagotto, Phys. Rev. B **103**, 045115 (2021).
[30] L.-F. Lin, N. Kaushal, Y. Zhang, A. Moreo, and E. Dagotto, Phys. Rev. Materials **5**, 025001 (2021).
[31] G. Grüner, *Density Waves in Solids* (Perseus, Cambridge, MA, 2000).
[32] Y. Zhang, L.-F. Lin, A. Moreo, S. Dong, and E. Dagotto, Phys. Rev. B **101**, 174106 (2020).
[33] E. Şaşıoğlu, C. Friedrich, and S. Blügel, Phys. Rev. B **83**, 121101(R) (2011).
[34] L. Vaugier, H. Jiang, and S. Biermann, Phys. Rev. B **86**, 165105 (2012).
[35] W. Witczak-Krempa, G. Chen, Y. B. Kim, and L. Balents, Annu. Rev. Condens. Matter Phys. **5**, 57 (2014).
[36] S. V. Streltsov and D. I. Khomskii, Phys. Rev. B **89**, 161112(R) (2014).
[37] Y. Zhang, L. F. Lin, A. Moreo, and E. Dagotto, Phys. Rev. B **104**, L060102 (2021).
[38] L. de' Medici, S. R. Hassan, M. Capone, and X. Dai, Phys. Rev. Lett. **102**, 126401 (2009).
[39] N. D. Patel, A. Nocera, G. Alvarez, A. Moreo, S. Johnston, and E. Dagotto, Commun. Phys. **2**, 64 (2019).
[40] J. Herbrych, J. Heverhagen, N. D. Patel, G. Alvarez, M. Daghofer, A. Moreo, and E. Dagotto, Phys. Rev. Lett. **123**, 027203 (2019).
[41] J. Herbrych, J. Heverhagen, N. D. Patel, G. Alvarez, M. Daghofer, A. Moreo, and E. Dagotto, Proc. Natl. Acad. Sci. USA **117**, 16226 (2020).
[42] B. J. Kim, H. Jin, S. J. Moon, J.-Y. Kim, B.-G. Park, C. S. Leem, J. Yu, T. W. Noh, C. Kim, S.-J. Oh, J.-H. Park, V. Durairaj, G. Cao, and E. Rotenberg, Phys. Rev. Lett. **101**, 076402 (2008).
[43] G. Jackeli and G. Khaliullin, Phys. Rev. Lett. **102**, 017205 (2009).
[44] C. Lu and J.-M. Liu, Adv. Mater. **32**, 1904508 (2019).
[45] A. Kitaev, Ann. Phys. (NY) **321**, 2 (2006).
[46] J. Chaloupka, G. Jackeli, and G. Khaliullin, Phys. Rev. Lett. **105**, 027204 (2010).

[47] Y. Singh, S. Manni, J. Reuther, T. Berlijn, R. Thomale, W. Ku, S. Trebst, and P. Gegenwart, Phys. Rev. Lett. **108**, 127203 (2012).

[48] S. K. Choi, R. Coldea, A. N. Kolmogorov, T. Lancaster, I. I. Mazin, S. J. Blundell, P. G. Radaelli, Y. Singh, P. Gegenwart, K. R. Choi, S.-W. Cheong, P. J. Baker, C. Stock, and J. Taylor, Phys. Rev. Lett. **108**, 127204 (2012).

[49] I. I. Mazin, H. O. Jeschke, K. Foyevtsova, R. Valenti, and D. I. Khomskii, Phys. Rev. Lett. **109**, 197201 (2012).

[50] J. G. Rau, E. K.-H. Lee, and H.-Y. Kee, Phys. Rev. Lett. **112**, 077204 (2014).

[51] J. Kim, J. Chaloupka, Y. Singh, J. W. Kim, B. J. Kim, D. Casa, A. Said, X. Huang, and T. Gog, Phys. Rev. X **10**, 021034 (2020).

[52] G. Bastien, G. Garbarino, R. Yadav, F. J. Martinez-Casado, R. Beltrán Rodríguez, Q. Stahl, M. Kusch, S. P. Limandri, R. Ray, P. Lampen-Kelley, D. G. Mandrus, S. E. Nagler, M. Roslova, A. Isaeva, T. Doert, L. Hozoi, A. U. B. Wolter, B. Büchner, J. Geck, and J. van den Brink, Phys. Rev. B **97**, 241108(R) (2018).

[53] G. Li, X. Chen, Y. Gan, F. Li, M. Yan, F. Ye, S. Pei, Y. Zhang, L. Wang, H. Su, J. Dai, Y. Chen, Y. Shi, X. W. Wang, L. Zhang, S. Wang, D. Yu, F. Ye, J.-W. Mei, and M. Huang, Phys. Rev. Materials **3**, 023601 (2019).

[54] K. W. Plumb, J. P. Clancy, L. J. Sandilands, V. V. Shankar, Y. F. Hu, K. S. Burch, H.-Y. Kee, and Y.-J. Kim, Phys. Rev. B **90**, 041112(R) (2014).

[55] R. D. Johnson, S. C. Williams, A. A. Haghighirad, J. Singleton, V. Zapf, P. Manuel, I. I. Mazin, Y. Li, H. O. Jeschke, R. Valentí, and R. Coldea, Phys. Rev. B **92**, 235119 (2015).

[56] A. Koitzsch, C. Habenicht, E. Müller, M. Knupfer, B. Büchner, H. C. Kandpal, J. van den Brink, D. Nowak, A. Isaeva, and T. Doert, Phys. Rev. Lett. **117**, 126403 (2016).

[57] H. B. Cao, A. Banerjee, J.-Q. Yan, C. A. Bridges, M. D. Lumsden, D. G. Mandrus, D. A. Tennant, B. C. Chakoumakos, and S. E. Nagler, Phys. Rev. B **93**, 134423 (2016).

[58] A. Banerjee, C. A. Bridges, J.-Q. Yan, A. A. Aczel, L. Li, M. B. Stone, G. E. Granroth, M. D. Lumsden, Y. Yiu, J. Knolle, S. Bhattacharjee, D. L. Kovrizhin, R. Moessner, D. A. Tennant, D. G. Mandrus, and S. E. Nagler, Nat. Mater. **15**, 733 (2016).

[59] Y. Kubota, H. Tanaka, T. Ono, Y. Narumi, and K. Kindo, Phys. Rev. B **91**, 094422 (2015).

[60] A. Glamazda, P. Lemmens, S.-H. Do, Y. S. Kwon, and K.-Y. Choi, Phys. Rev. B **95**, 174429 (2017).

[61] H.-S. Kim, V. V. Shankar, C. Andrei, and H.-Y. Kee, Phys. Rev. B **91**, 241110(R) (2015).

[62] Y. S. Hou, H. J. Xiang, and X. G. Gong, Phys. Rev. B **96**, 054410 (2017).

[63] C. Eichstaedt, Y. Zhang, P. Laurell, S. Okamoto, A. G. Eguiluz, and T. Berlijn, Phys. Rev. B **100**, 075110 (2019).

[64] S.-H. Baek, S.-H. Do, K.-Y. Choi, Y. S. Kwon, A. U. B. Wolter, S. Nishimoto, J. van den Brink, and B. Buchner, Phys. Rev. Lett. **119**, 037201 (2017).

[65] J. Zheng, K. Ran, T. Li, J. Wang, P. Wang, B. Liu, Z.-X. Liu, B. Normand, J. Wen, and W. Yu, Phys. Rev. Lett. **119**, 227208 (2017).

[66] Y. Kasahara, K. Sugii, T. Ohnishi, M. Shimozawa, M. Yamashita, N. Kurita, H. Tanaka, J. Nasu, Y. Motome, T. Shibauchi, and Y. Matsuda, Phys. Rev. Lett. **120**, 217205 (2018).

[67] S.-H. Do, S.-Y. Park, J. Yoshitake, J. Nasu, Y. Motome, Y. S. Kwon, D. T. Adroja, D. J. Voneshen, K. Kim, T.-H. Jang, J.-H. Park, K.-Y. Choi, and S. Ji, Nat. Phys. **13**, 1079 (2017).

[68] A. Banerjee, J. Yan, J. Knolle, C. A. Bridges, M. B. Stone, M. D. Lumsden, D. G. Mandrus, D. A. Tennant, R. Moessner, and S. E. Nagler, Science **356**, 1055 (2019).

[69] A. Banerjee, P. Lampen-Kelley, J. Knolle, C. Balz, A. A. Aczel, B. Winn, Y. Liu, D. Pajerowski, J. Yan, C. A. Bridges, A. T. Savici, B. C. Chakoumakos, M. D. Lumsden, D. A. Tennant, R. Moessner, D. G. Mandrus, and S. E. Nagler, npj Quantum Mater. **3**, 8 (2018).

[70] Y. Kasahara, T. Ohnishi, Y. Mizukami, O. Tanaka, S. Ma, K. Sugii, N. Kurita, H. Tanaka, J. Nasu, Y. Motome, T. Shibauchi, and Y. Matsuda, Nature (London) **559**, 227 (2018).

[71] D. Ni, X. Gui, K. M. Powderly, and R. J. Cava, Adv. Mater. 2106831 (2022).

[72] K. Nawa, Y. Imai, Y. Yamaji, H. Fujihara, W. Yamada, R. Takahashi, T. Hiraoka, M. Hagihala, S. Torii, T. Aoyama, T. Ohashi, Y. Shimizu, H. Gotou, M. I Itoh, K. Ohgushi, and T. J. Sato, J. Phys. Soc. Jpn. **90**, 123703 (2021).

[73] C. Huang, J. Zhou, H. Wu, K. Deng, P. Jena, and E. Kan, Phys. Rev. B **95**, 045113 (2017).

[74] F. Ersan, E. Vatansever, S. Sarikurt, Y. Yüksel, Y. Kadioglu, H. D. Ozaydin, O. Aktürk, Ü. Akıncı, and E. Aktürk, J. Magn. Magn. Mater. **476**, 111 (2019).

[75] G. Kresse and J. Hafner, Phys. Rev. B **47**, 558 (1993).

[76] G. Kresse and J. Furthmüller, Phys. Rev. B **54**, 11169 (1996).

[77] P. E. Blöchl, Phys. Rev. B **50**, 17953 (1994).

[78] J. P. Perdew, K. Burke, and M. Ernzerhof, Phys. Rev. Lett. **77**, 3865 (1996).

[79] L. Chaput, A. Togo, I. Tanaka, and G. Hug, Phys. Rev. B **84**, 094302 (2011).

[80] A. Togo and I. Tanaka, Scr. Mater. **108**, 1 (2015).

[81] S. L. Dudarev, G. A. Botton, S. Y. Savrasov, C. J. Humphreys, and A. P. Sutton, Phys. Rev. B **57**, 1505 (1998).

[82] H.-S. Kim and H.-Y. Kee, Phys. Rev. B **93**, 155143 (2016).

[83] R. I. Eglitis, J. Purans, and R. Jia, Crystals **11**, 455 (2021).

[84] R. I. Eglitis, J. Purans, A. I. Popov, and R. Jia, Symmetry **13**, 1920 (2021).

[85] K. Momma and F. Izumi, J. Appl. Crystallogr. **44**, 1272 (2011).

[86] J. P. Perdew, A. Ruzsinszky, G. I. Csonka, O. A. Vydrov, G. E. Scuseria, L. A. Constantin, X. Zhou, and K. Burke, Phys. Rev. Lett. **100**, 136406 (2008).

[87] S. Grimme, J. Antony, S. Ehrlich, and S. Krieg, J. Chem. Phys. **132**, 154104 (2010).

[88] S. Grimme, S. Ehrlich, and L. Goerigk, J. Comput. Chem. **32**, 1456 (2011).

[89] See Supplemental Material at http://link.aps.org/supplemental/10.1103/PhysRevB.105.085107 for more results, including phonon spectrum with $U_{\text{eff}} = 2$ eV and electronic structures different phases of α-$RuCl_3$ or α-RuI_3.

[90] A. Savin, O. Jepsen, J. Flad, O.-K. Andersen, H. Preuss, and H. G. von Schnering, Angew. Chem., Int. Ed. **31**, 187 (1992).

[91] I. Pollini, Phys. Rev. B **53**, 12769 (1996).

[92] L. Binotto, I. Pollini, and G. Spinolo, Phys. Status Solidi B **44**, 245 (1970).

[93] L. J. Sandilands, Y. Tian, A. A. Reijnders, H.-S. Kim, K. W. Plumb, Y.-J. Kim, H.-Y. Kee, and K. S. Burch, Phys. Rev. B **93**, 075144 (2016).